arXiv:1403.0972v2 [cond-mat.mtrl-sci] 5 Aug 2014

Molecular weight dependent bimolecular recombination in organic solar cells

Bronson Philippa,[1] Martin Stolterfoht,[2] Ronald D. White,[1] Marrapan Velusamy,[2] Paul L. Burn,[2] Paul Meredith,[2] and Almantas Pivrikas[2]

[1]*School of Engineering and Physical Sciences, James Cook University, Townsville 4811, Australia*

[2]*Centre for Organic Photonics & Electronics (COPE), School of Chemistry and Molecular Biosciences and School of Mathematics and Physics, The University of Queensland, Brisbane 4072, Australia*

Abstract

Charge carrier recombination is studied in operational organic solar cells made from the polymer:fullerene system PCDTBT:PC71BM (poly[*N*-9”-heptadecanyl-2,7-carbazole-*alt*-5,5-(4’,7’-di-2-thienyl-2’,1’,3’-benzothiadiazole)] : [6,6]-phenyl-C_{70}-butyric acid methyl ester). A newly developed technique High Intensity Resistance dependent PhotoVoltage (HI-RPV) is presented for reliably quantifying the bimolecular recombination coefficient independently of variations in experimental conditions, thereby resolving key limitations of previous experimental approaches. Experiments are performed on solar cells of varying thicknesses and varying polymeric molecular weights. It is shown that solar cells made from low molecular weight PCDTBT exhibit Langevin recombination, whereas suppressed (non-Langevin) recombination is found in solar cells made with high molecular weight PCDTBT.

I. INTRODUCTION

Bimolecular recombination is one of the key loss mechanisms in organic bulk heterojunction solar cells, especially in thicker devices or those made from materials which do not possess a sufficiently high carrier mobility[1–3]. Recombination coefficients are commonly compared with the prediction of Langevin [2, 4, 5], i.e. $\beta_{\mathrm{L}} = e\left(\mu_{\mathrm{p}} + \mu_{\mathrm{n}}\right)/\varepsilon\varepsilon_0$, where e is the charge of an electron, μ_{p} (μ_{n}) is the mobility of holes (electrons), and $\varepsilon\varepsilon_0$ is the dielectric permittivity. A suppressed, non-Langevin recombination coefficient (with $\beta < \beta_L$) has been reported in organic photovoltaic blends that exhibit high performance [6–10]. Suppressed recombination is desirable to ensure efficient charge extraction. The reduction factor β/β_L is a useful "figure of merit" for screening candidate photovoltaic blends to rapidly identify those which are likely to be highly performing [4].

A variety of techniques are available to study recombination dynamics. Techniques that operate on fully operational devices (i.e. those without blocking layers or other modifications[11]) include transient photovoltage (TPV) [12, 13], photogenerated charge extraction by linearly increasing voltage (photo-CELIV) [14, 15], and time-of-flight (TOF) [16, 17].

TPV studies often show an apparent reaction order higher than the expected value of two [18]. It has been suggested that this is due to a concentration dependence in the recombination coefficient [19], recombination through trap states[20], or the spatial separation of the carriers under open circuit conditions [18]. The spatial separation at open-circuit conditions can be reduced by studying the solar cell nearer to short-circuit conditions, as in the photo-CELIV or TOF experiments.

Photo-CELIV can be used to study charge carrier mobility and also the bimolecular recombination coefficient [21–26]. The recombination coefficient can be estimated from the maximum extraction current in the photo-CELIV transient[27, 28]. However, this transient is influenced by experimental factors that are not fully accounted for in the theory, such as the spatial distribution of light absorption[28], the circuit resistance[29], and the voltage slope[30]. Additionally, premature escape of charge from the film[31] contributes to the charge redistribution during the delay time[32], which results in a false position of the extraction maximum and makes the measurement unreliable. While some attention has been directed to minimizing this issue[33], a full compensation of carrier redistribution is impossible due to Fermi level pinning, an inhomogeneous electric field inside the film and strong diffusion near the electrode where carriers are photogenerated.

Another well known technique to characterise recombination is high intensity time-of-flight (TOF)[34–36]. The recombination coefficient can be estimated from the amount of charge extracted during a TOF experiment[4, 37, 38]. However, the external circuit resistance influences the extracted charge[9], making the measurement unreliable due to its dependence on the experimental conditions. Previous works have neglected the impact of the *RC* circuit [4]. Here, we resolve this issue by extending the previous work to achieve more reliable experimental results.

In this article, we study recombination in the benchmark organic photovoltaic system PCDTBT:PC71BM (see the experimental section for details of the materials). We quantify the recombination in this system, and compare solar cells made with low molecular weight PCDTBT to those made with high molecular weight PCDTBT. Our recombination study will be conducted using a variant of time-of-flight that we call High Intensity Resistance dependent PhotoVoltage (HI-RPV). An exact analytic solution of the relevant differential equations is not known, so we apply numerical simulations to show the applicability of the technique to a variety of experimental conditions [29, 39–43]. The details of our numerical solver are presented in Appendix A. After demonstrating the generality of the technique, we go on to apply it to operational bulk heterojunction solar cells.

II. EXPERIMENTAL SETUP

The experimental setup is shown in Figure 1. Similarly with time-of-flight, charges are photogenerated using a high intensity laser, and the voltage across the load resistor is measured with an oscilloscope. However, in contrast with traditional time-of-flight, the measurement is repeated many times across a wide range of load resistances. Furthermore, volume photogeneration is desirable, and consequently operational thin-film solar cells can be studied.

The experiment begins with the photogeneration of a large quantity ($\gg CU$) of charge carriers using an intense laser pulse. These carriers induce a photocurrent that charges the electrodes, which act as capacitive plates. The electrodes rapidly acquire a charge of CU, where C is the capacitance and U is the solar cell's built in field (or the applied voltage). Next, two processes occur simultaneously. The first is the recombination of the photogenerated charges, and the second is the discharge of the capacitor through the external *RC* circuit. If the *RC* time is large, then the photocarriers will completely recombine before the capacitor can discharge. Regardless of the nature of the recombination, one can always find a resistance R large enough that the *RC* time

greatly exceeds the lifetime of charge carriers. Consequently, in the limit of large R, the extracted charge will be limited to CU. Conversely, if the RC time is small, then the capacitor will discharge before the carriers completely recombine, more photocurrent will flow, and the extracted charge will exceed CU. In the intermediate regime, there is an interplay between the bimolecular lifetime and the RC time. We exploit this relationship in order to quantify the carrier recombination.

III. DEVICE THICKNESS AND LIGHT ABSORPTION PROFILE

The simulated impact of light intensity and the optical absorption (or photogeneration) profile is shown in Figure 2. We applied the Beer-Lambert law to represent the photogeneration profile,

$$n_0 = p_0 = L\alpha e^{-\alpha x}, \tag{1}$$

where n_0 (p_0) is the initial concentration of electrons (holes), L is the light intensity in photons per unit area, α is the absorption coefficient at the laser wavelength, and x is the spatial coordinate. The other simulation settings are given in Appendix B.

Figure 2 shows that the extracted charge Q_e/CU becomes essentially independent of αd when αd is less than 1, where d is the device thickness. The inset of Figure 2 shows the αd dependence at high light intensity, demonstrating that Q_e/CU is essentially insensitive to the initial carrier spatial distribution, in the case of volume generation. For example, in the case of $\alpha d = 3$ (see Figure 2), the light intensity at the back of the device is approximately 5% of the light intensity at the front of the device. Such a strong inhomogeneity in the spatial distribution does not meaningfully affect the extracted charge.

Physically, the insignificance of the initial spatial distribution is caused by bimolecular recombination. The bimolecular recombination process will be more rapid in regions of higher light intensity, and slower in regions of lower light intensity. This will, in effect, "smooth" the carrier distribution across the device, erasing the initial spatial distribution. More precisely, the carrier concentration at early times is given by $n(t) = \left(n_0^{-1} + \beta t\right)^{-1}$, where n_0 is the initial carrier concentration [44]. In the limit of very large n_0, the dependence on the initial condition vanishes [$n(t) \approx (\beta t)^{-1}$]. This explains why the absorption profile is irrelevant at high light intensities.

In summary, to first order, detailed optical modelling to account for exact carrier distribution in operational solar cells is not necessary, since the precise spatial distribution of carriers is rapidly erased by bimolecular recombination. Therefore, the HI-RPV technique can be applied to thin

film devices ($\alpha d \leq 1$) without concern for optical interference.

Since the technique is insensitive to the light absorption profile, we will remove αd from the set of parameters being tested, and approximate the initial condition by perfectly uniform carrier generation. All subsequent numerical calculations are performed with this simplified uniform initial condition, rather than the Beer-Lambert law.

IV. CIRCUIT RESISTANCE

In a HI-RPV experiment, the circuit resistance is varied over many orders of magnitude in order to observe the dynamical interaction between the known circuit *RC* time and the unknown bimolecular lifetime.

We examined the impact of the circuit resistance using our simulations, as shown in Figure 3. Importantly, we observe that more charge can be extracted at lower resistances. A smaller resistance allows the charge extraction to complete in a shorter time, so that less recombination occurs, and the overall extracted charge is higher.

The faster carrier mobility is normalised out of the simulation by the system of units (as described in Appendix A). However, it is necessary to specify the ratio of carrier mobilities $\mu_{\text{faster}}/\mu_{\text{slower}}$. To confirm that variation in this ratio will not interfere with the measurement, Figure 3 shows the case of balanced mobilities ($\mu_{\text{faster}}/\mu_{\text{slower}} = 1$) with filled symbols and lines and strongly unbalanced mobilities ($\mu_{\text{faster}}/\mu_{\text{slower}} = 100$) with open symbols and no lines. This covers a wide range of mobility ratios to examine the variation that might be expected to occur in practice. The two cases (balanced mobilities and strongly unbalanced mobilities) are essentially indistinguishable, as shown in Figure 3. We explain this insensitivity as follows. The amount of extracted charge Q_{e} is primarily controlled by the recombination. The Langevin recombination rate is proportional to the *sum* of carrier mobilities. The relevant time scale for this process is $t_{\text{tr(sum)}} \equiv d^2/\left(\mu_{\text{p}} + \mu_{\text{n}}\right) U$.

Figure 3 shows that the extracted charge saturates at high light intensities to a value that we call $Q_{e(\text{sat})}/CU$, as indicated by the arrows. Therefore, if the HI-RPV experiment is operated in this saturation regime, the amount of extracted charge does not depend on the laser power which is applied. The extracted charge is also independent of the carrier mobility ratio (Figure 3) and the light absorption profile (Figure 2). Consequently, the only parameters remaining to be quantified are the circuit resistance and the bimolecular recombination coefficient.

The impact of the circuit resistance is shown in Figure 4. If the normalised resistance is small, the extracted charge $Q_{e(sat)}$ can exceed the charge on the electrodes CU by an order of magnitude or more, even in the presence of Langevin recombination. The TOF experiment under these circumstances is therefore misleading, especially if comparing two systems with different values of the normalised resistance, $RC/t_{tr(sum)}$. We resolve this problem by introducing the HI-RPV technique. We firstly develop predictions for Langevin systems, and then in the following section extend this to the general case.

Figure 4 shows a single universal curve that all Langevin systems should obey. We developed an empirical equation to describe this curve by arbitrarily choosing an appropriate functional form that would give a logarithmic dependence at small R (as shown in Figure 4), and would saturate to 1 at large R (as also shown in Figure 4),

$$\frac{Q_{e(sat)}}{CU} = 1 + p_1 \log\left[1 + p_2 \left(\frac{t_{tr(sum)}}{RC}\right)^{p_3}\right]. \tag{2}$$

We used non-linear least squares regression to calculate the coefficients p_i from the simulation results in Figure 4. The result is:

$$\frac{Q_{e(sat)}}{CU} = 1 + 1.8 \log\left[1 + 0.63 \left(\frac{t_{tr(sum)}}{RC}\right)^{0.55}\right], \tag{3}$$

which is valid for Langevin recombination and thin films. Equation (3) is plotted against the simulation results in Figure 4, demonstrating excellent agreement.

The purpose of Eq. (3) is to determine the type of recombination present in a thin film device; for example, one could plot this equation alongside measured data in order to determine whether the recombination is of the Langevin type. This is important, since recombination orders higher than two have been experimentally observed [18], and it is necessary to identify the type of recombination dynamics that might apply to the system being studied. A plot of extracted charge versus resistance (Figure 4) will follow the form of Eq. (3) if Langevin recombination is dominant. In contrast, if there is a higher order of recombination, then the carrier concentration will decay according to a different time dependence, and the functional form of the extracted charge versus resistance will change. If the recombination is stronger than Langevin, the experimental data will lie *below* the line. On the other hand, if the dominant form of recombination is slower than Langevin, then less recombination will occur and the experimental data will lie *above* the line.

We will show below that our experimental data can be described by a bimolecular recombination process with a Langevin reduction prefactor. We do not exclude the possibility of higher-order effects such as a concentration-dependent recombination coefficient [19], but these are not necessary to explain our data. Therefore, in the following section, we extend our theory to systems with suppressed (non-Langevin) recombination of purely second order.

V. BIMOLECULAR RECOMBINATION COEFFICIENT

In order to develop a tool for convenient experimental quantification of the recombination coefficient (β/β_L), we applied numerical simulations to predict the amount of extracted charge as a function of β/β_L. These simulations are plotted in Figure 5. As expected, the amount of extracted charge increases dramatically in the presence of non-Langevin recombination. To confirm that our technique remains valid, we checked that non-Langevin devices also exhibit saturation at high light intensity, and that the extracted charge is independent of the optical absorption profile for thin films ($\alpha d < 1$). We found that systems with strongly suppressed recombination ($\beta \ll \beta_{\mathrm{L}}$) exhibit a stronger dependence on the mobility ratio than Langevin systems. The more unbalanced the mobilities, the less charge can be extracted. A representative example ($\mu_{\mathrm{faster}}/\mu_{\mathrm{slower}} = 10$) is plotted in Figure 5 with open symbols.

We are now ready to specify how the HI-RPV technique can be applied. The recombination coefficient can be determined by comparing measurements of the extracted charge against the simulation results in Figure 5. This approach is valid for any thin film ($\alpha d < 1$) device. Importantly, this technique is not hindered by the RC-dependence that affects traditional high intensity TOF [4, 9], because the impact of the RC time constant on the extracted charge is accounted for on the horizontal axis of Figure 5. However, for accurate measurements, it is necessary to reach the regime where $RC/t_{\mathrm{tr(sum)}} \ll 1$. This may not be possible in extremely high mobility materials, especially when the series resistances are included in R. Ideally, R should be varied over many orders of magnitude.

As an alternative to visual inspection of the graph, we can also specify an empirical equation that describes the data in Figure 5. We started with the general functional form [Eq. (2)] and applied a procedure similar to that described earlier for the Langevin case. With least squares regression, we found the parameters p_i as a function of β/β_{L}. Finally, we parametrised the p_i

values as follows, choosing an arbitrary functional form that best described the data:

$$p_1 = 1.829\left(\frac{\beta}{\beta_L} + 0.0159\sqrt{\frac{\beta}{\beta_L}}\right)^{-1} \quad (4)$$

$$p_2 = 0.63\left(\frac{\beta}{\beta_L}\right)^{0.407} \quad (5)$$

$$p_3 = 0.55\left(\frac{\beta}{\beta_L}\right)^{0.0203}. \quad (6)$$

These functional forms were found to obtain the best fit to the simulated results.

Figure 5 shows the simulation results compared with Eq. (2) with the parameters (4)-(6). A good agreement is demonstrated for balanced mobilities; if the mobilities are unbalanced then Eq. (2) will slightly overestimate the extracted charge.

These equations are a convenient tool to analyse experimental data. For example, to determine the recombination coefficients for the data presented below, we set up a spreadsheet table to compare the model with experimental data and thereby estimate the bimolecular recombination coefficient.

In order to confirm the validity of the newly presented HI-RPV technique, we have compared its results in various systems with other techniques including photo-CELIV, double injection transients, plasma extraction, and steady-state IVs. The results are in agreement, given the limitations of each technique. These limitations must be carefully considered when comparing measurements, which is why we have developed the present HI-RPV approach.

VI. EXPERIMENTAL MEASUREMENTS

We manufactured bulk heterojunction solar cells with the donor:acceptor blend poly[*N*-9”-heptadecanyl-2,7-carbazole-*alt*-5,5-(4’,7’-di-2-thienyl-2’,1’,3’-benzothiadiazole)] (PCDTBT) and [6,6]-phenyl-C_{71}-butyric acid methyl ester (PC70BM). This blend, PCDTBT:PC70BM, has previously been reported to exhibit near to Langevin recombination[36]. Two sources of PCDTBT were used. A low molecular weight batch ($\overline{M}_n$ = 4.3 kDa, $\overline{M}_w$ = 12.1 kDa, PDI = 2.8, obtained in 1,2,4-trichlorobenzene at 140 °C) was synthesized in our laboratory following the Suzuki cross-coupling protocols previously described[45]. A high molecular weight batch ($\overline{M}_n$ = 22.7 kDa, $\overline{M}_w$ = 122.2 kDa, PDI = 5.4) was purchased from the SJPC Group.

The fabrication of the solar cells followed a previously described procedure[46]. 15 Ω/sq. Indium Tin Oxide (ITO) coated glass substrates patterned by photolithography (Kintec) were

cleaned by sonicating in sequence with alconox (detergent), de-ionised water, acetone, and *iso*-propanol for 10 minutes. The cleaned substrates were coated with a 20 nm layer of poly(3,4-ethylenedioxythiophene):poly(styrene sulfonate) (PEDOT:PSS) by spin casting at 5000 rpm for 60 sec. The PEDOT:PSS layer was baked for 10 minutes at 170 °C. A solution of PCDTBT and commercially purchased PC70BM (Nano-C) with a mass ratio of 1:4 was prepared at a total concentration of 20 mg/mL in anhydrous 1,2-dichlorobenzene. This solution was deposited by spin coating on top of the PEDOT:PSS layer after filtration. Two substrates were prepared from the low molecular weight batch with active layer thicknesses of 46 nm and 130 nm, respectively. From the high molecular weight batch, two additional substrates were made with active layer thicknesses of 75 nm and 90 nm. Thicknesses were measured by a Veeco Dektak150 profilometer. Slow drying was performed after spin coating by placing the coated film in a partially opened petri dish for 2 hours. Finally, a 100 nm aluminium layer was deposited by thermal evaporation under a 10^{-6} mbar vacuum. The device areas were 0.035 cm^2 with three devices per substrate. The low molecular weight material produces solar cells with power conversion efficiencies (PCE) of approximately 4%; whereas optimised solar cells made from the high molecular weight material have PCEs in excess of 6%[47]. Transit times were measured using low light intensity resistance dependent photovoltage [48]; the mobilities were $\mu_{\text{low MW}} \approx 8 \times 10^{-5}\,\text{cm}^2\text{V}^{-1}\text{s}^{-1}$ and $\mu_{\text{high MW}} \approx 2 \times 10^{-3}\,\text{cm}^2\text{V}^{-1}\text{s}^{-1}$, demonstrating greatly improved charge transport in the latter devices. Further work would be needed to identify the underlying mechanism for this change. We note that a strong dependence of mobility on molecular weight has been observed in other polymers in the past [49].

HI-RPV measurements were performed using a pulsed third-harmonic Nd:YAG laser (Quantel Brio) working at a wavelength of 355 nm and pulse duration of 5 ns. At 355 nm, the absorption coefficient of this blend[50] is 8×10^4 cm^{-1}, which gives αd values of 0.37 for the thinnest device (46 nm) and 1.0 for the thickest device (130 nm). The laser beam was attenuated using a neutral density filter set. No external voltage was applied; instead, the transients were driven by the solar cells' built-in field. The signal was recorded by a digital storage oscilloscope (LeCroy Waverunner A6200).

We performed HI-RPV with load resistances in the range from 1 Ω to 1 MΩ. The results are plotted in Figure 6. This graph demonstrates the application of the HI-RPV technique. It is important to note that the resistance value R on the horizontal axis is the *complete* circuit resistance, calculated as the sum of the load resistance and the solar cell series resistance. The experimental

data is plotted together with the predicted curve from Eq. (2) with parameters (4)-(6). The measured extracted charge behaves as expected and as predicted by the simulations. The extracted charge decreases with increasing resistance until it saturates to $Q_{e(sat)}/CU = 1$. To determine the recombination strength, the coefficient β/β_L was adjusted until the predicted curves matched the experimental data.

Our results indicate that low molecular weight devices exhibit Langevin-type recombination, while the high molecular weight devices exhibit non-Langevin recombination with $\beta/\beta_L \approx 0.07$. Photo-CELIV measurements applied to the same devices demonstrated Langevin and non-Langevin recombination, respectively, supporting our results. However, photo-CELIV is subject to various limitations, as we discussed in the Introduction, and so we developed HI-RPV for the detailed study. The strong change in the recombination strength likely contributes to the improved power conversion efficiency of the high molecular weight blend. It has previously been reported that PCDTBT solar cell performance improves with increasing molecular weight[51]. Our results indicate that suppressed recombination may be the mechanism behind this performance trend, and hence the molecular weight is a parameter that should be considered when optimising solar cell performance. There may be further performance improvements to be gained by identifying the molecular weight at which the recombination is minimised.

A previous study of recombination in PCDTBT solar cells[36] reported reduction factors in the range of $\beta/\beta_L = 0.3$ to $\beta/\beta_L = 1$ depending upon the device thickness. Thinner devices were reported to exhibit more strongly reduced recombination. Thickness dependencies cannot be reliably studied using time-of-flight because variations in the thickness influence parameters such as the device capacitance, the *RC* time, the transit time, the optical absorption profile, and the amount of extracted charge. Consequently, with time-of-flight it is difficult to eliminate the dependence on the experimental parameters. In contrast, HI-RPV accounts for these effects. We did not observe any thickness dependence, although the range of thicknesses measured here is less than that in the previous study[36].

Further work is necessary in order to clarify the origin of this molecular weight dependence, as well as any dependence on other parameters such as polydispersity, impurity density, and conjugation length. The novel HI-RPV technique will be beneficial for such future work.

VII. CONCLUSION

We studied recombination in the organic photovoltaic system PCDTBT:PC70BM, and observed that devices made with a higher molecular weight polymer exhibit suppressed recombination relative to devices made with a lower molecular weight polymer. Our results highlight the importance of material quality for fabrication of high efficiency organic solar cells. We developed and implemented a theoretical framework for the novel High Intensity Resistance dependent PhotoVoltage (HI-RPV) technique, which allows recombination measurements that are independent of the experimental conditions, resolving a key weakness of previous time-of-flight based techniques. A key advantage of HI-RPV is its independence on the light absorption profile in thin films, making it applicable to operational devices.

Acknowledgements

We thank Anton Bavdek for helpful assistance with the experimental work. We thank the James Cook University High Performance Computing Centre for computational resources. A.P. is the recipient of an Australian Research Council Discovery Early Career Researcher Award (Projects: ARC DECRA DE120102271, UQ ECR59-2011002311 and UQ NSRSF-2011002734). P.M. and P.L.B. are UQ Vice Chancellor's Senior Research Fellows. B.P. is funded by an Australian Postgraduate Award (APA). M.S. is funded by a University of Queensland International scholarship (UQI). We acknowledge funding from the University of Queensland (Strategic Initiative - Centre for Organic Photonics & Electronics), the Queensland Government (National and International Research Alliances Program) and the ARC Centre of Excellence for Antimatter-Matter Studies. This work was performed in part at the Queensland node of the Australian National Fabrication Facility (ANFF-Q) - a company established under the National Collaborative Research Infrastructure Strategy to provide nano and microfabrication facilities for Australia's researchers.

Appendix A: Numerical Drift-Diffusion Solver

Our simulations take an effective medium approach to model device-scale behaviour, an approach which is commonly used for organic solar cell simulation [29, 39–43]. We consider the situation where the films are not doped and there is no film charging due to deep traps whose release times are longer than the transit time. These assumptions are typically met in high efficiency

devices.

We apply one dimensional continuity equations for electron and hole number densities[29, 39, 40, 52, 53]. These are coupled to the Poisson equation, to incorporate the effects of space charge. All quantities are scaled such that they are dimensionless. We denote dimensionless quantities with a prime. The non-dimensionalisation is similar to that used by Juška *et al*[54, 55].

The length scale is the film thickness: $x' \equiv x/d$. The time scale is the transit time calculated for the fastest mobility: $t' \equiv t/t_{\mathrm{tr}}$. The voltage scale is the applied voltage: $U' \equiv U/U_{\mathrm{applied}}$. This system of units requires that the normalised faster carrier mobility is $\mu'_{\mathrm{faster}} = 1$.

The charge scale is the charge on the electrodes: $Q' \equiv Q/CU$. The number density scale is CU per volume: $n' \equiv enSd/CU$, where S is the surface area of the device. The current scale is CU per transit time: $j' \equiv jt_{tr}/CU$. The circuit resistance is expressed internally in the simulations by $R' \equiv RC/t_{\mathrm{tr}}$, but everywhere in this article, we present it instead as $R' \equiv RC/t_{\mathrm{tr(sum)}}$. This is because the scaling with respect to the *sum* of mobilities eliminates most of the mobility ratio dependence in Q_{e}, as shown in Figure 3.

The Einstein relation for diffusion gives a dimensionless temperature $T' = kT/eU_{\mathrm{applied}}$. The recombination coefficient is normalised to the Langevin rate: $\beta' \equiv \beta/\beta_L$.

The model equations for the semiconductor bulk are:

$$j'_{\mathrm{p}} = \mu'_{\mathrm{p}} E' p' - \mu'_{\mathrm{p}} T' \frac{\partial p'}{\partial x'} \tag{A1}$$

$$j'_{\mathrm{n}} = \mu'_{\mathrm{n}} E' n' + \mu'_{\mathrm{n}} T' \frac{\partial n'}{\partial x'} \tag{A2}$$

$$\frac{\partial p'}{\partial t'} + \frac{\partial j'_{\mathrm{p}}}{\partial x'} = -\beta' \left(\mu'_{\mathrm{p}} + \mu'_{\mathrm{n}}\right) n' p' \tag{A3}$$

$$\frac{\partial n'}{\partial t'} - \frac{\partial j'_{\mathrm{n}}}{\partial x'} = -\beta' \left(\mu'_{\mathrm{p}} + \mu'_{\mathrm{n}}\right) n' p' \tag{A4}$$

$$\frac{\partial^2 U'}{\partial \left(x'\right)^2} = n' - p' \tag{A5}$$

$$E' = -\frac{\partial U'}{\partial x'}. \tag{A6}$$

The boundary conditions for Poisson's equation are:

$$U'(t,0) = V' \tag{A7}$$

$$U'(t,1) = 0, \tag{A8}$$

where V' is the voltage across the semiconductor:

$$\frac{dV'}{dt'} = \frac{1-V'}{R'} - j'_{\mathrm{c}} \tag{A9}$$

$$j'_{\mathrm{c}} = \int_0^1 j'_{\mathrm{p}}(x) + j'_{\mathrm{n}}(x)\, dx. \tag{A10}$$

The boundary conditions for the number density are as follows. We use a finite volume method, so the boundary conditions for the transport equations are expressed in terms of the fluxes j'_{p} and j'_{n} at each electrode. Since the RPV experiment is conducted under reverse bias, we assume no injection is possible. This immediately sets two such edge fluxes to zero. The other two represent charge *extraction* and are described by the local drift current $j'_{\mathrm{p}} = \mu'_{\mathrm{p}} E' p'$ (and similarly for electrons).

The initial condition for the number density is Eq. (1) in normalised units:

$$n'(0,x') = p'(0,x') = L'\alpha' e^{-\alpha' x'}, \tag{A11}$$

with $Q'_{\mathrm{ph}} = L'\left(1-e^{-\alpha'}\right)$; or alternatively, by the condition of uniform generation

$$n'(0,x') = p'(0,x') = Q'_{\mathrm{ph}}. \tag{A12}$$

The initial condition for voltage is $V' = 1$.

The spatial discretisation of these equations was performed using the finite volume method. Number densities are defined at cell midpoints, whereas the fluxes and the electric field are defined on the cell boundaries. This results in a large system of coupled ODEs in time. We implemented these in Matlab, and found that the *ode15s* solver usually provides the best performance out of all the standard Matlab ODE solvers.

Appendix B: Simulation settings for Figure 2

The light intensity is represented by the quantity of photogenerated charge carriers $Q_{\mathrm{ph}} = L\left(1-e^{-\alpha d}\right)$, which is the integral of Eq. (1) over the device. We selected a fixed circuit resistance, $RC/t_{\mathrm{tr(sum)}} = 0.05$, where R is the resistance of the circuit external to the device, C is the device capacitance, and $t_{\mathrm{tr(sum)}} \equiv d^2\left(\mu_{\mathrm{p}}+\mu_{\mathrm{n}}\right)^{-1}U^{-1}$ is an effective transit time calculated from the sum of carrier mobilities crossing a film of thickness d under a voltage U. The bimolecular recombination was given by the Langevin rate ($\beta/\beta_L = 1$). The simulations were conducted with

equal electron and hole mobilities; however, the results are essentially unchanged if the mobilities are not equal (as shown in Figure 3).

---

[1] P. W. M. Blom, V. D. Mihailetchi, L. J. A. Koster, and D. E. Markov, Advanced Materials **19**, 1551 (2007).

[2] C. Deibel and V. Dyakonov, Reports on Progress in Physics **73**, 096401 (2010).

[3] A. Pivrikas, H. Neugebauer, and N. S. Sariciftci, IEEE Journal of Selected Topics in Quantum Electronics **16**, 1746 (2010).

[4] A. Pivrikas, G. Juška, A. J. Mozer, M. Scharber, K. Arlauskas, N. S. Sariciftci, H. Stubb, and R. Österbacka, Physical Review Letters **94**, 176806 (2005).

[5] A. Pivrikas, N. S. Sariciftci, G. Juška, and R. Österbacka, Progress in Photovoltaics: Research and Applications **15**, 677 (2007).

[6] G. Juska, K. Arlauskas, J. Stucklik, and R. Osterbacka, Journal of Non-Crystalline Solids **352**, 1167 (2006).

[7] C. G. Shuttle, A. Maurano, R. Hamilton, B. OâĂŹRegan, J. C. de Mello, and J. R. Durrant, Applied Physics Letters **93**, 183501 (2008).

[8] L. J. A. Koster, M. Kemerink, M. M. Wienk, K. Maturová, and R. A. J. Janssen, Advanced Materials **23**, 1670 (2011).

[9] T. M. Clarke, J. Peet, P. Denk, G. Dennler, C. Lungenschmied, and A. J. Mozer, Energy & Environmental Science **5**, 5241 (2012).

[10] H. Azimi, T. Heumüller, A. Gerl, G. Matt, P. Kubis, M. Distaso, R. Ahmad, T. Akdas, M. Richter, W. Peukert, and C. J. Brabec, Advanced Energy Materials **3**, 1589 (2013).

[11] G.-J. A. H. Wetzelaer, N. J. Van der Kaap, L. J. A. Koster, and P. W. M. Blom, Advanced Energy Materials **3**, 1130 (2013).

[12] C. Shuttle, B. O'Regan, A. Ballantyne, J. Nelson, D. Bradley, and J. Durrant, Physical Review B **78**, 113201 (2008).

[13] C. G. Shuttle, B. O'Regan, A. M. Ballantyne, J. Nelson, D. D. C. Bradley, J. de Mello, and J. R. Durrant, Applied Physics Letters **92**, 093311 (2008).

[14] G. Juška, K. Arlauskas, M. Viliunas, and J. Kočka, Physical Review Letters **84**, 4946 (2000).

[15] A. J. Mozer, N. S. Sariciftci, L. Lutsen, D. Vanderzande, R. OĬĹsterbacka, M. Westerling, and

G. JusÌŇka, Applied Physics Letters **86**, 112104 (2005).

[16] W. Spear, Journal of Non-Crystalline Solids **1**, 197 (1969).

[17] W. Spear, Advances in Physics **23**, 523 (1974).

[18] T. Kirchartz and J. Nelson, Physical Review B **86**, 165201 (2012).

[19] A. Maurano, R. Hamilton, C. G. Shuttle, A. M. Ballantyne, J. Nelson, B. O'Regan, W. Zhang, I. McCulloch, H. Azimi, M. Morana, C. J. Brabec, and J. R. Durrant, Advanced Materials **22**, 4987 (2010).

[20] A. Foertig, J. Rauh, V. Dyakonov, and C. Deibel, Physical Review B **86**, 115302 (2012).

[21] G. Adam, A. Pivrikas, A. M. Ramil, S. Tadesse, T. Yohannes, N. S. Sariciftci, and D. A. M. Egbe, Journal of Materials Chemistry **21**, 2594 (2011).

[22] D. A. M. Egbe, E. Tekin, E. Birckner, A. Pivrikas, N. S. Sariciftci, and U. S. Schubert, Macromolecules **40**, 7786 (2007).

[23] D. A. M. Egbe, G. Adam, A. Pivrikas, A. M. Ramil, E. Birckner, V. Cimrova, H. Hoppe, and N. S. Sariciftci, Journal of Materials Chemistry **20**, 9726 (2010).

[24] N. Yilmaz Canli, S. Günes, A. Pivrikas, A. Fuchsbauer, D. Sinwel, N. Sariciftci, O. Yasa, and B. Bilgin-Eran, Solar Energy Materials and Solar Cells **94**, 1089 (2010).

[25] S. Günes, A. Wild, E. Cevik, A. Pivrikas, U. S. Schubert, and D. A. Egbe, Solar Energy Materials and Solar Cells **94**, 484 (2010).

[26] C. Vijila, S. P. Singh, E. Williams, P. Sonar, A. Pivrikas, B. Philippa, R. White, E. Naveen Kumar, S. Gomathy Sandhya, S. Gorelik, J. Hobley, A. Furube, H. Matsuzaki, and R. Katoh, Journal of Applied Physics **114**, 184503 (2013).

[27] N. Nekrašas, K. Genevičius, M. ViliÅńnas, and G. Juška, Chemical Physics **404**, 56 (2012).

[28] G. Juška, N. Nekrašas, V. Valentinavičius, P. Meredith, and A. Pivrikas, Physical Review B **84**, 155202 (2011).

[29] M. Neukom, N. Reinke, and B. Ruhstaller, Solar Energy **85**, 1250 (2011).

[30] J. Lorrmann, B. H. Badada, O. Inganäs, V. Dyakonov, and C. Deibel, Journal of Applied Physics **108**, 113705 (2010).

[31] R. Österbacka, G. JusÌŇka, K. Arlauskas, A. J. Pal, K.-M. KaÌĹllman, and H. Stubb, Journal of Applied Physics **84**, 3359 (1998).

[32] G. Sliaužys, G. Juška, K. Arlauskas, A. Pivrikas, R. Österbacka, M. Scharber, A. Mozer, and N. Sariciftci, Thin Solid Films **511-512**, 224 (2006).

[33] A. Baumann, J. Lorrmann, D. Rauh, C. Deibel, and V. Dyakonov, Advanced Materials **24**, 4381

(2012).

[34] S. Tiwari and N. C. Greenham, Optical and Quantum Electronics **41**, 69 (2009).

[35] A. Kokil, K. Yang, and J. Kumar, Journal of Polymer Science Part B: Polymer Physics **50**, 1130 (2012).

[36] T. M. Clarke, J. Peet, A. Nattestad, N. Drolet, G. Dennler, C. Lungenschmied, M. Leclerc, and A. J. Mozer, Organic Electronics **13**, 2639 (2012).

[37] A. Pivrikas, G. Juška, R. Österbacka, M. Westerling, M. Viliunas, K. Arlauskas, and H. Stubb, Physical Review B **71**, 125205 (2005).

[38] C. Vijila, A. Pivrikas, H. Chun, C. Zhikuan, R. Osterbacka, and C. Jin, Organic Electronics **8**, 8 (2007).

[39] L. Koster, E. Smits, V. Mihailetchi, and P. Blom, Physical Review B **72**, 085205 (2005).

[40] I. Hwang, C. R. McNeill, and N. C. Greenham, Journal of Applied Physics **106**, 094506 (2009).

[41] M. Neukom, S. Züfle, and B. Ruhstaller, Organic Electronics **13**, 2910 (2012).

[42] R. C. I. MacKenzie, C. G. Shuttle, M. L. Chabinyc, and J. Nelson, Advanced Energy Materials **2**, 662 (2012).

[43] R. Hanfland, M. A. Fischer, W. BruÌĹtting, U. WuÌĹrfel, and R. C. I. MacKenzie, Applied Physics Letters **103**, 063904 (2013).

[44] M. A. Lampert and P. Mark, *Current injection in solids* (Academic Press, 1970).

[45] N. Blouin, A. Michaud, D. Gendron, S. Wakim, E. Blair, R. Neagu-Plesu, M. Belletête, G. Durocher, Y. Tao, and M. Leclerc, Journal of the American Chemical Society **130**, 732 (2008).

[46] A. Armin, G. Juška, B. W. Philippa, P. L. Burn, P. Meredith, R. D. White, and A. Pivrikas, Advanced Energy Materials **3**, 321 (2013).

[47] A. K. Pandey, M. Aljada, M. Velusamy, P. L. Burn, and P. Meredith, Advanced Materials **24**, 1055 (2012).

[48] B. Philippa, M. Stolterfoht, P. L. Burn, G. Juška, P. Meredith, R. D. White, and A. Pivrikas, Submitted to Physical Review B (2013).

[49] R. Kline, M. McGehee, E. Kadnikova, J. Liu, and J. Fréchet, Advanced Materials **15**, 1519 (2003).

[50] S. H. Park, A. Roy, S. Beaupré, S. Cho, N. Coates, J. S. Moon, D. Moses, M. Leclerc, K. Lee, and A. J. Heeger, Nature Photonics **3**, 297 (2009).

[51] S. Wakim, S. Beaupré, N. Blouin, B.-R. Aich, S. Rodman, R. Gaudiana, Y. Tao, and M. Leclerc, Journal of Materials Chemistry **19**, 5351 (2009).

[52] I. Hwang and N. C. Greenham, Nanotechnology **19**, 424012 (2008).

[53] J. Rogel-Salazar, D. D. C. Bradley, J. R. Cash, and J. C. Demello, Physical Chemistry Chemical Physics **11**, 1636 (2009).

[54] G. Juška, M. Viliunas, O. Klíma, E. Šípek, and J. Kočka, Philosophical Magazine Part B **69**, 277 (1994).

[55] G. Juška, M. Viliunas, K. Arlauskas, and J. Kočka, Physical Review B **51**, 16668 (1995).

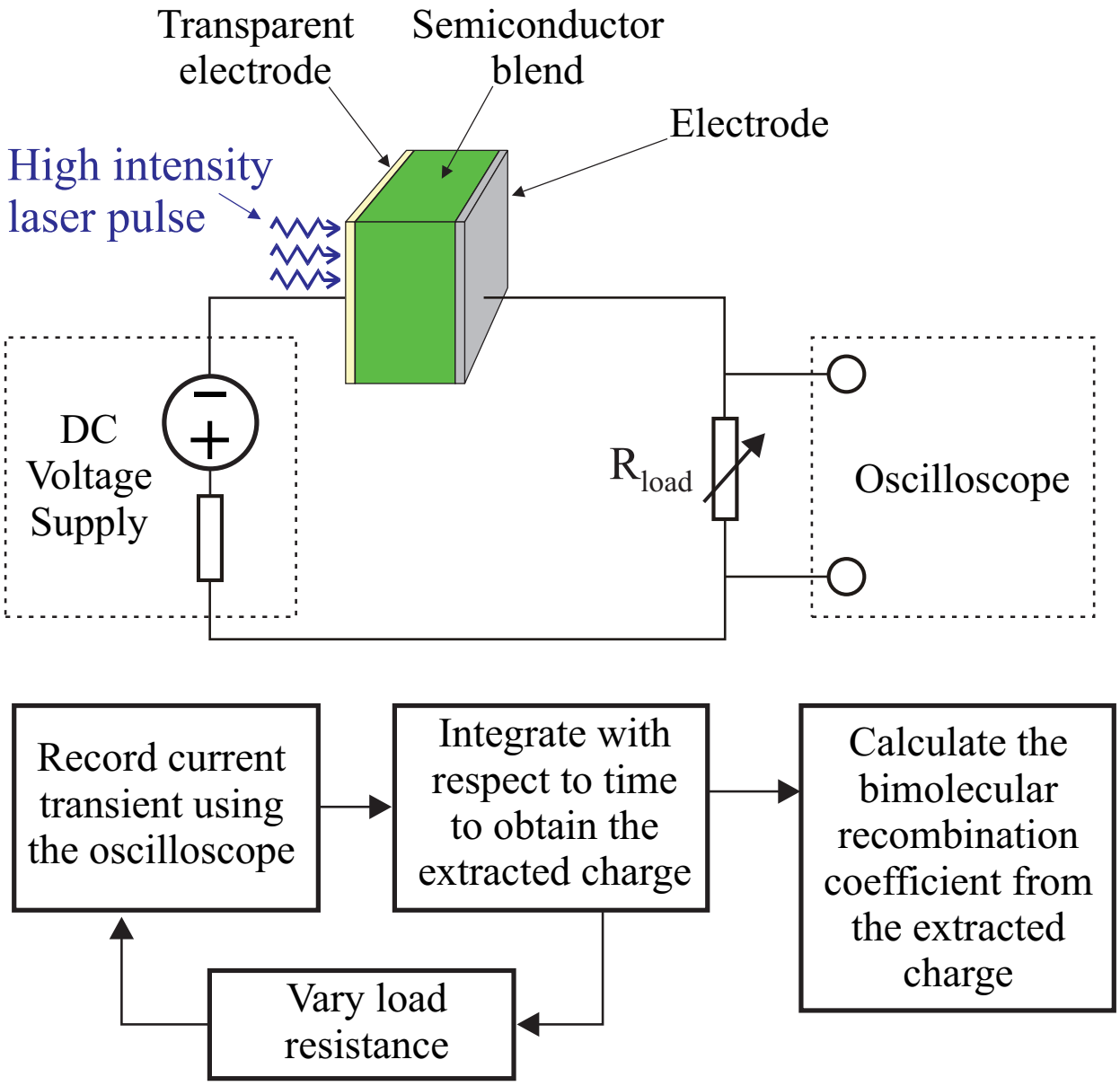

Figure 1: Circuit schematic for the High Intensity Resistance dependent PhotoVoltage (HI-RPV) experiment. Current transients are recorded across a range of load resistances, and then integrated to obtain the extracted charge, Q_e. The variation in the extracted charge with resistance is used to quantify the recombination processes and determine the bimolecular recombination coefficient. If the device under test is an operational solar cell, then the DC voltage supply is optional and the experiment can be done under the solar cell's built-in field.

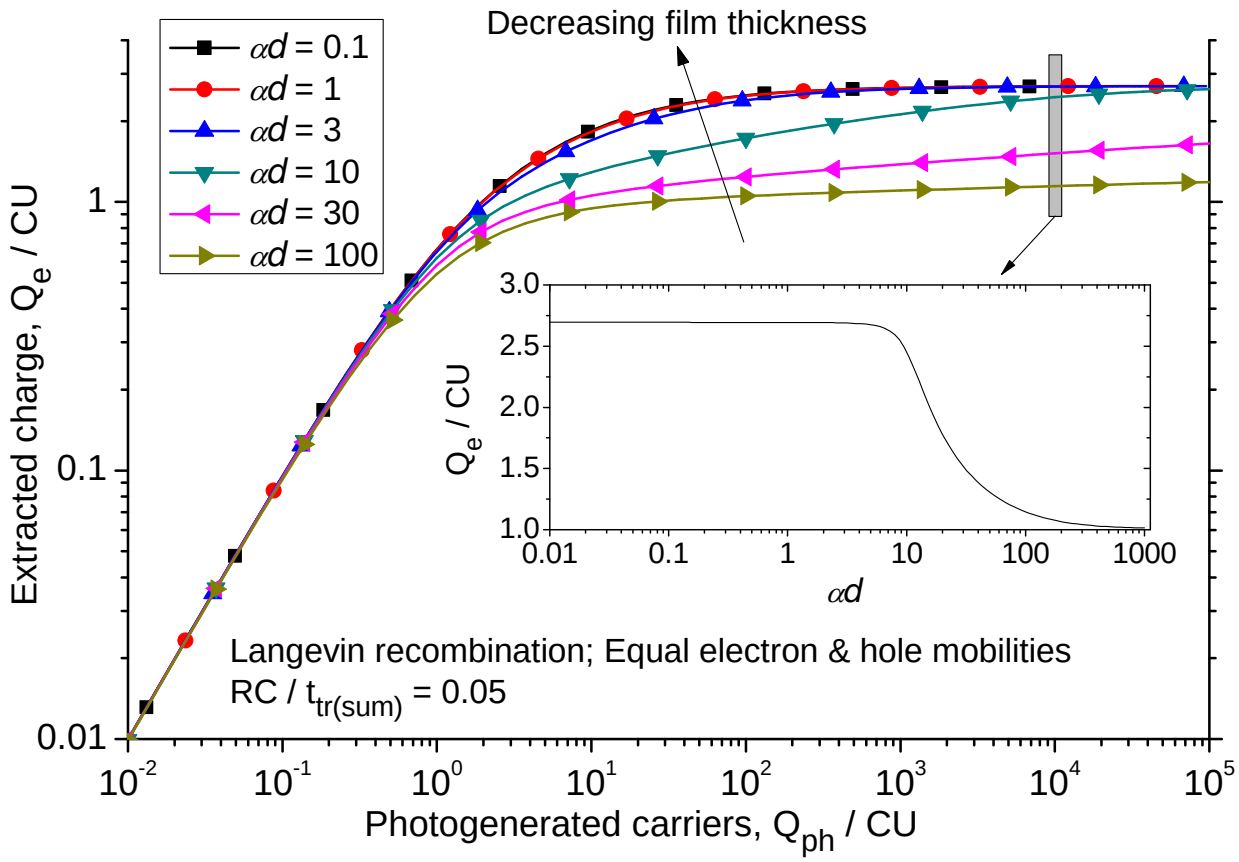

Figure 2: The impact of the film thickness and light absorption profile on the extracted charge. The film thickness is incorporated within the absorption-thickness product αd (where α is the absorption coefficient and d the thickness). The inset shows the αd dependence in the region indicated by the thin grey box ($Q_{ph}/CU = 10^4$), and demonstrates that the extracted charge is independent of the initial carrier distribution for thin films ($\alpha d < 1$). The extracted charge readily saturates with high light intensity. This graph shows that a general theory for thin film devices can be developed, without detailed optical modelling, and without regard for the precise quantity of photogenerated carriers in the saturation regime.

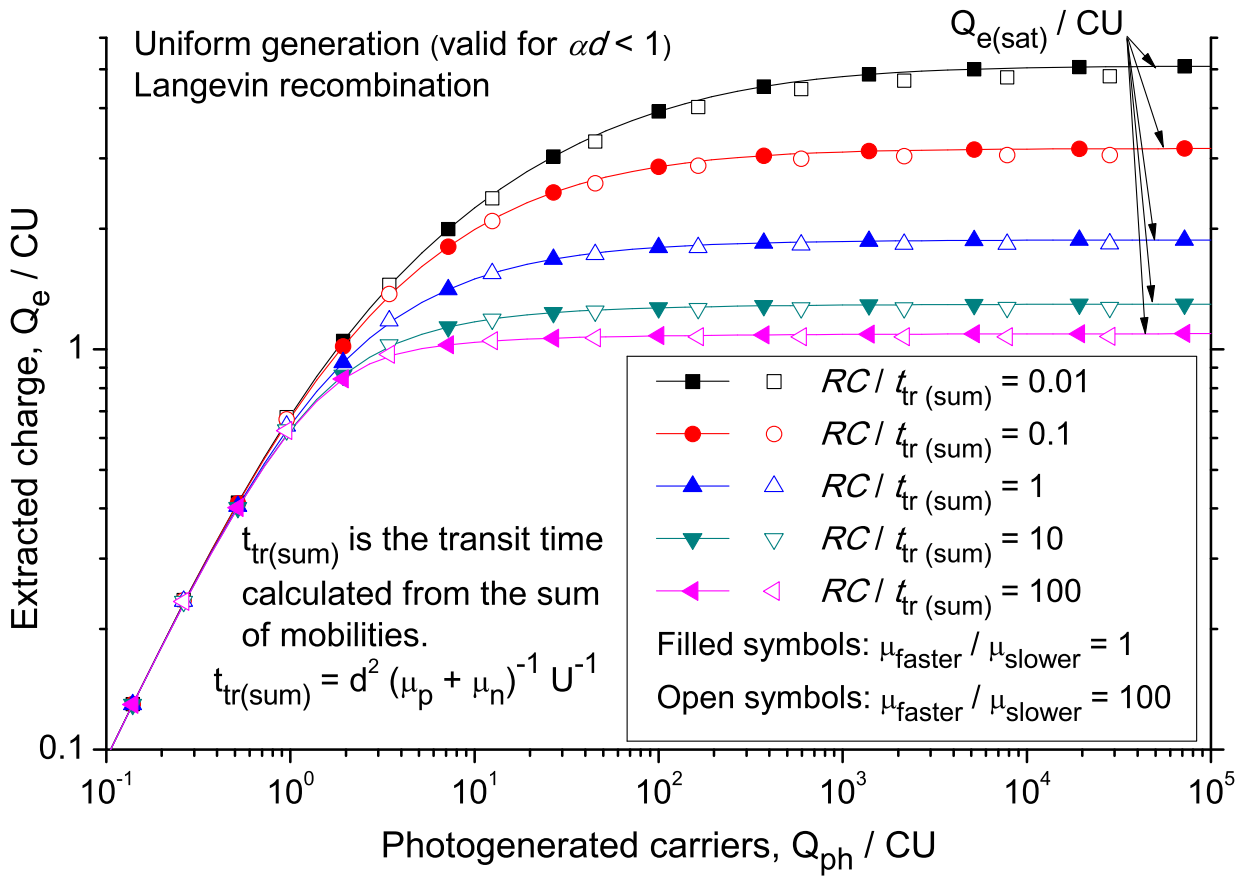
Uniform generation (valid for $\alpha d < 1$)
Langevin recombination
$Q_{e(sat)}$ / CU
$t_{tr(sum)}$ is the transit time calculated from the sum of mobilities.
$t_{tr(sum)} = d^2 (\mu_p + \mu_n)^{-1} U^{-1}$
$RC / t_{tr\ (sum)}$ = 0.01
$RC / t_{tr\ (sum)}$ = 0.1
$RC / t_{tr\ (sum)}$ = 1
$RC / t_{tr\ (sum)}$ = 10
$RC / t_{tr\ (sum)}$ = 100
Filled symbols: $\mu_{faster} / \mu_{slower}$ = 1
Open symbols: $\mu_{faster} / \mu_{slower}$ = 100
Extracted charge, Q_e / CU
Photogenerated carriers, Q_{ph} / CU
0.1
1
10^{-1}
10^{0}
10^{1}
10^{2}
10^{3}
10^{4}
10^{5}

Figure 3: The impact of the circuit resistance on the extracted charge from simulated resistance dependent photovoltage experiments. Filled symbols with lines show balanced mobilities ($\mu_{\text{faster}}/\mu_{\text{slower}} = 1$); open symbols without lines show strongly unbalanced mobilities ($\mu_{\text{faster}}/\mu_{\text{slower}} = 100$). The two are very similar, because the normalisation scale for the circuit *RC* time minimises the effect of the mobility ratio. The saturation value $Q_{e(sat)}/CU$ depends almost entirely upon the normalised resistance. These results demonstrate that the load resistance needs to be accounted for to correctly measure the recombination coefficient.

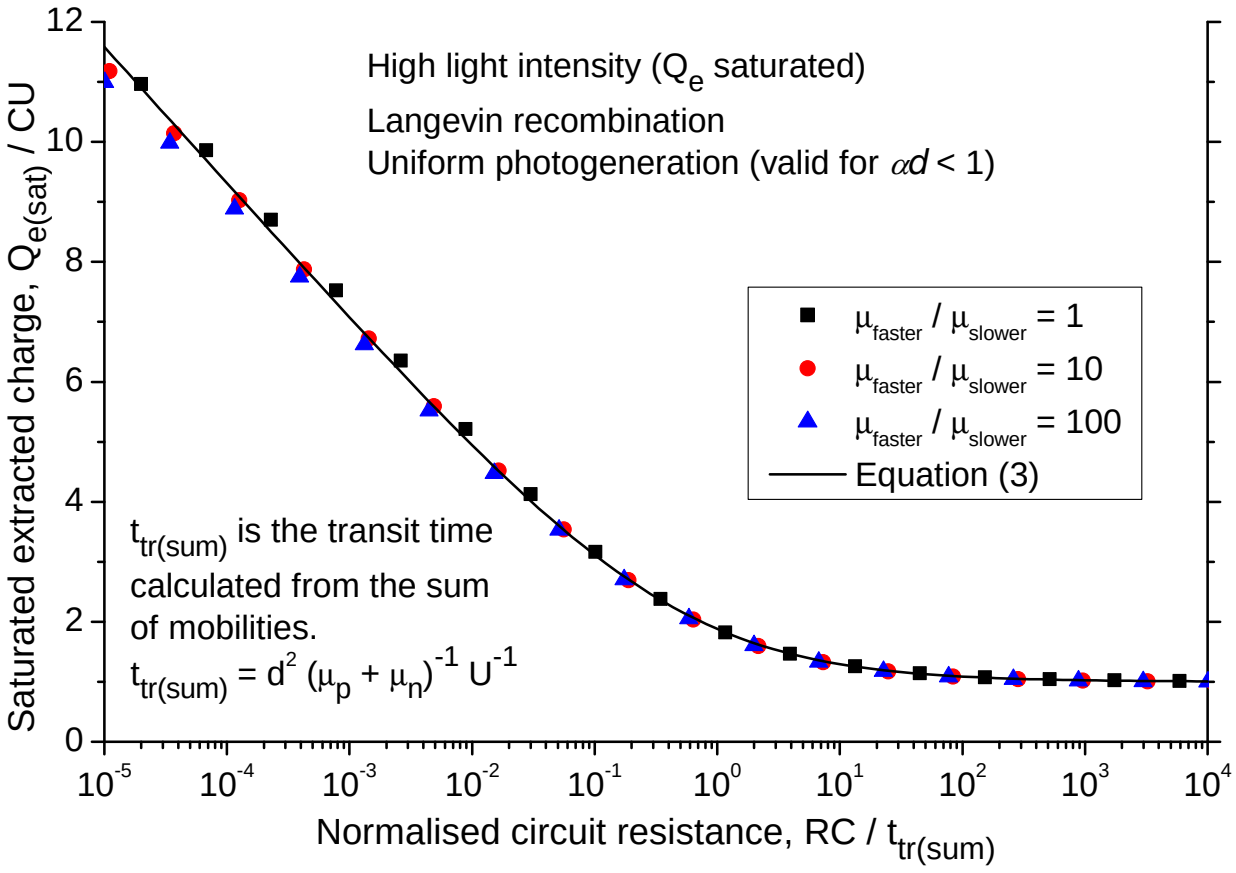

Figure 4: Simulations of the impact of load resistance on the extracted charge from thin film devices with Langevin recombination at varying mobility ratios. Points are calculated from simulations at high light intensity ($Q_{ph}/CU = 10^6$, although the precise value is unimportant because of the saturation in the extracted charge Q_e, as shown in Figure 3). The ratio of carrier mobilities does not affect the extracted charge, so HI-RPV measurements can be applied equally to systems with balanced mobilities and systems with strongly unbalanced mobilities.

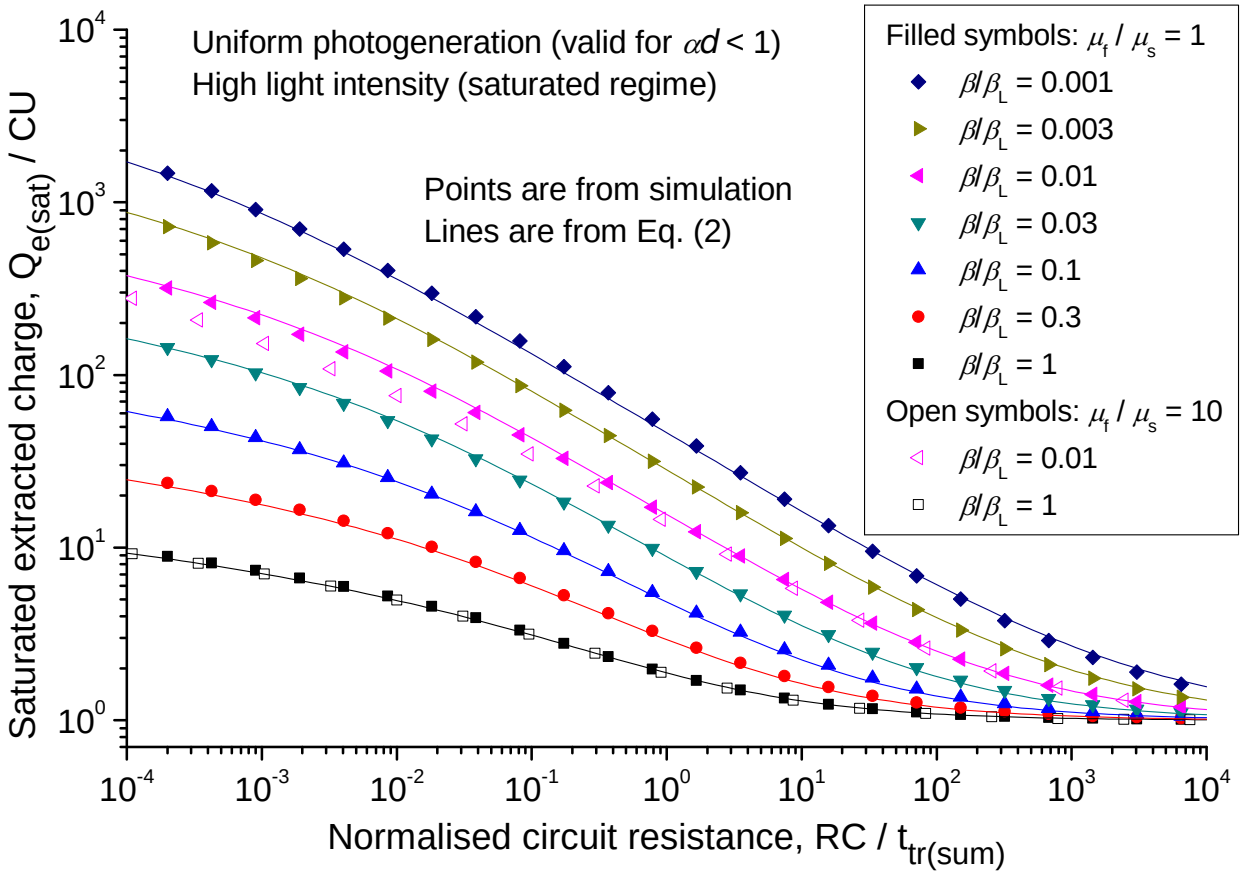
Uniform photogeneration (valid for αd < 1)
High light intensity (saturated regime)
Points are from simulation
Lines are from Eq. (2)
Filled symbols: μf / μs = 1
β/βL = 0.001
β/βL = 0.003
β/βL = 0.01
β/βL = 0.03
β/βL = 0.1
β/βL = 0.3
β/βL = 1
Open symbols: μf / μs = 10
β/βL = 0.01
β/βL = 1
Saturated extracted charge, Qe(sat) / CU
Normalised circuit resistance, RC / ttr(sum)

Figure 5: Numerically predicted extracted charge as a function of load resistance in high light intensity resistance dependent photovoltage (HI-RPV) experiments for different recombination coefficients β/β_L. The extracted charge shown in this figure is calculated at the highest light intensities where the extracted charge saturates, as shown in Fig. 2. The points are from simulations, whereas the lines are Eq. (2) evaluated for each respective value of β/β_L. This graph presents numerical predictions to be used when measuring the recombination coefficient β/β_L experimentally from HI-RPV in systems without deep traps.

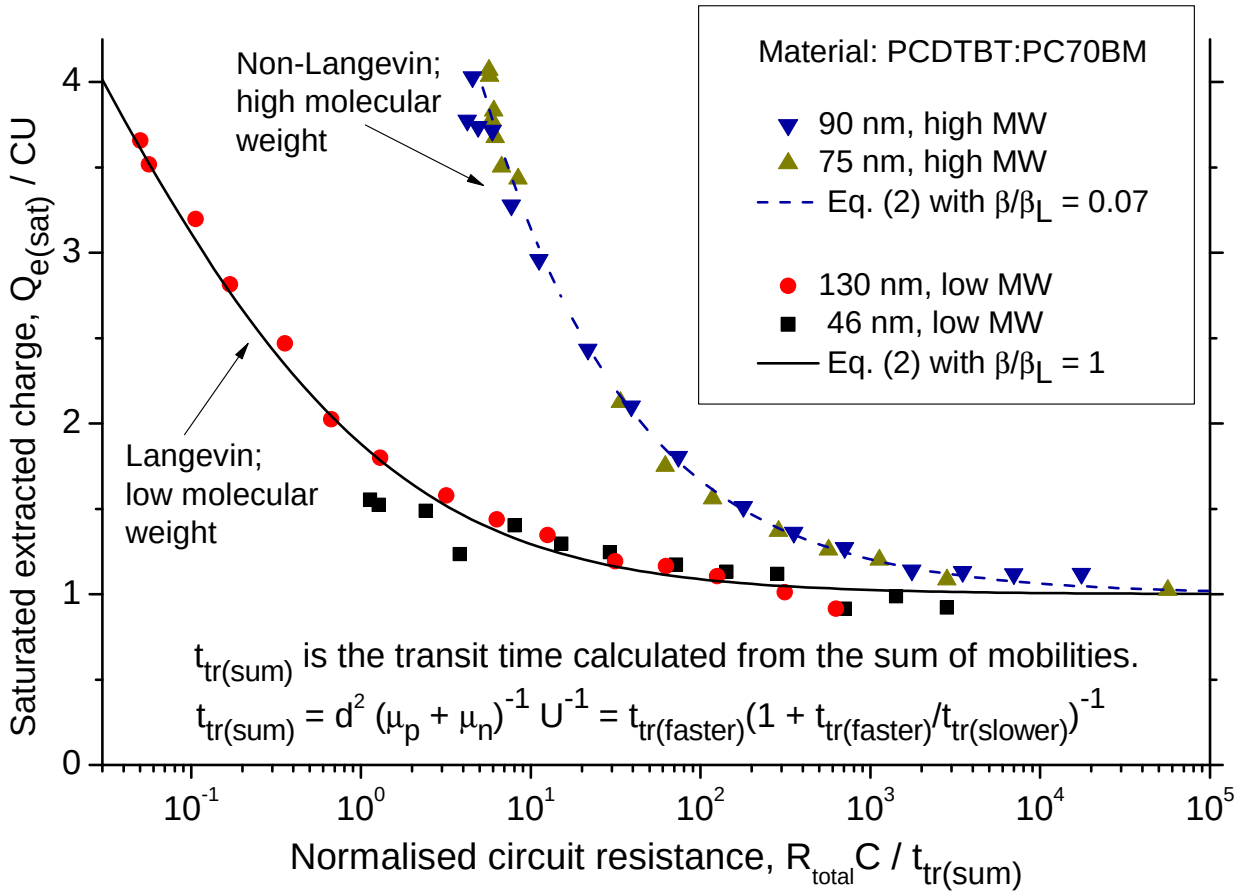

Figure 6: Experimentally measured extracted charge as a function of circuit resistance obtained using the HI-RPV technique. Films made with the low molecular weight polymer exhibit Langevin recombination, whereas films containing the high molecular weight polymer exhibit suppressed non-Langevin recombination. Non-Langevin recombination is beneficial to solar cell performance, indicating the importance of material quality in device fabrication.